Electronic Supplementary Information

Triptycene-fused multi-resonance TADF material endows high-efficiency electroluminescence and low efficiency roll-off

Ke-Ke Tan,[a,b] Meng Li*[,a,b] and Chuan-Feng Chen*[a,b]

[a]*Beijing National Laboratory for Molecular Sciences, CAS Key Laboratory of Molecular Recognition and Function, Institute of Chemistry, Chinese Academy of Sciences, Beijing 100190, China.*

[b]*University of Chinese Academy of Sciences, Beijing 100049, China.*

E-mail: cchen@iccas.ac.cn; limeng@iccas.ac.cn.

Contents

1. General information

All the reagents were purchased from commercial sources and used without further purification. ^{1}H and ^{13}C NMR spectra were recorded on AVIII 500 MHz NMR spectrometers in $CDCl_3$ solutions. High-resolution mass spectra were measured on a Thermo Fisher® Exactive high resolution LC-MS spectrometer. The calculation was carried out with the Gaussian 09 software package.[S1] Geometry optimizations were conducted under the B3LYP/6-311g(d) level of theory. The ground state geometry of **TpBN** were optimized by density functional theory (DFT) using the B3LYP functional. The thermogravimetric analysis (TGA) was performed on a Q600 SDT thermal analyzer at a heating rate of 10°C min^{-1} in nitrogen, and differential scanning calorimetric (DSC) were performed on a Q2000 at a heating rate of 10°C min^{-1} in nitrogen. Cyclic voltammetry was performed using a CHI600A analyzer with a scan rate of 100 MV s^{-1} at room temperature to investigate the oxidation potentials. A conventional three electrodes cell was used as electrolytic cell with a glassy carbon working electrode, an Ag/Ag^{+} (0.01 M $AgNO_3$) as the reference electrode, and Pt wire as the counter electrode. The oxidation potential was measured in CH_2Cl_2 with 0.1 M of tetra-*n*-butylammonium hexafluorophosphate (*n*-Bu_4NPF_6) as a supporting electrolyte. Ferrocene used as internal standard for calibrating the reference electrode. UV-Vis spectra were recorded on PerkinElmer® UV/Vis/NIR spectrometer (Lambda 950). The photoluminescence spectra and transient PL decay characteristics were measured on an Edinburgh Instruments FLS 1000 spectrometer. Absolute photoluminescence quantum yields (PLQYs) was measured on HORIBA Fluorescence spectrometer.

The OLED devices were fabricated by vacuum deposition onto pre-coated ITO glass substrates at a low pressure (1×10^{-5} mbar) for organic and metal deposition successively Indium tin oxide (ITO) coated glass with a sheet resistance of 10 Ω per square was used as the anode substrate. Before the fabrication of devices, the ITO glass substrates were cleaned with Decon 90, rinsed in ultrapure water and ethanol, dried in an oven at 110 °C, and finally treated with O_2 plasma for 2 minutes. The electroluminescence and current-voltage-luminance characteristics of the devices were measured with a computer-controlled Spectrascan PR 670 spectrophotometer and Keithley 2400 SourceMeter after device pack

2. Synthesis, NMR spectra and high-resolution mass spectrometry

2.1 Synthesis

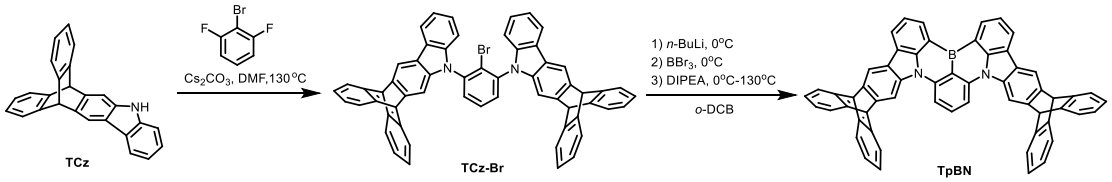

Scheme S1. Synthetic route of **TpBN**.

Synthesis of TCz-Br: The **TCz** (2.33 mmol, 800 mg), 1-bromo-2,6-difluorobenzene (0.58 mmol, 112 mg) and Cs_2CO_3 (4.65 mmol, 1517 mg) were dissolved in mixed solution of dimethylformamide (10 mL), the mixture was stirred for 24 h at 130°C under N_2 atmosphere. After cooling to room temperature, the mixture was extracted with CH_2Cl_2, and then the mixture was concentrated to obtain the yellow crude compound. And then, reflux the crude compound in methanol for 5 h. Filter while hot to afford white powder (310 mg, 64% yield).

^{1}H NMR (500 MHz, $CDCl_3$): δ 8.13 (d, *J* = 5.1 Hz, 2H), 8.05 (t, *J* = 8.1 Hz, 2H), 7.71–7.66 (m, 1H), 7.58 (t, *J* = 7.8 Hz, 2H), 7.49–7.38 (m, 9H), 7.35 (d, *J* = 7.3 Hz, 1H), 7.30 (d, *J* = 12.7 Hz, 2H), 7.21–7.15 (m, 2H), 7.11–6.93 (m, 10H), 5.60 (d, *J* = 12.2 Hz, 2H), 5.55 (s, 1H), 5.48 (s, 1H). ^{13}C NMR (125 MHz, $CDCl_3$): δ146.0, 145.9, 145.7, 145.6, 145.3, 145.1, 145.1, 143.9, 143.9,140.9, 140.8, 139.3, 139.3, 138.6, 138.6, 137.8, 131.1, 131.0, 129.3, 125.4, 125.3, 125.3, 125.2, 125.1, 125.1, 125.1, 123.7, 123.7, 123.6, 123.6, 123.5, 123.5, 123.5, 120.3, 120.2, 120.0, 115.5, 110.1, 110.1, 106.1, 54.7, 54.6, 54.1, 54.1. HR-MS (APCI): *m/z* calcd for $C_{52}H_{28}N_6$ $[M+H]^+$ 839.2056, found 839.2082.

Synthesis of TpBN: Add **TCz-Br** (2.38 mmol, 2.00 g) and *o*-DCB (30 mL) to the Schlenk flask under N_2 atmosphere. Then, adding *n*-BuLi (4.76 mmol, 1.9 mL, 2.5 M hexane solution) in an ice water bath. After stirring at room temperature for 5 hours, slowly add BBr_3 (4.76 mmol, 1.20 g) at 0°C, and then stir the mixture at room temperature for 5 hours. *N*, *N*-diisopropylethylamine (9.53 mmol, 1.23 g) was added at 0°C. Then heat the reaction mixture to 130°C and stir for 24 hours. Further purification was carried out by column chromatography on silica gel using CH_2Cl_2/petroleum ether (1:5, v/v) as the eluent to afford yellow powder (491 mg, 27% yield).

^{1}H NMR (500 MHz, $CDCl_3$): δ 8.70 (d, *J* = 7.1 Hz, 2H), 7.95 (s, 2H), 7.79–7.56 (m, 13H), 7.51 (s, 3H), 7.20–7.07 (m, 9H), 5.61 (s, 2H), 5.54 (s, 2H). ^{13}C NMR (125 MHz, $CDCl_3$): δ 145.7, 145.6, 145.1, 143.6, 143.2, 142.4, 138.6, 137.9, 136.6, 132.5, 132.3, 129.7, 129.0, 128.6, 128.2, 126.4, 125.4, 125.3, 123.9,

123.8, 123.6, 123.4, 123.2, 123.0, 122.8, 121.1, 115.3, 110.6, 108.2, 55.1, 53.7. HR-MS (APCI): *m/z* calcd for $C_{58}H_{34}BN_2^+$ $[M+H]^+$ 769.2810, found 769.2801.

2.2. NMR spectra

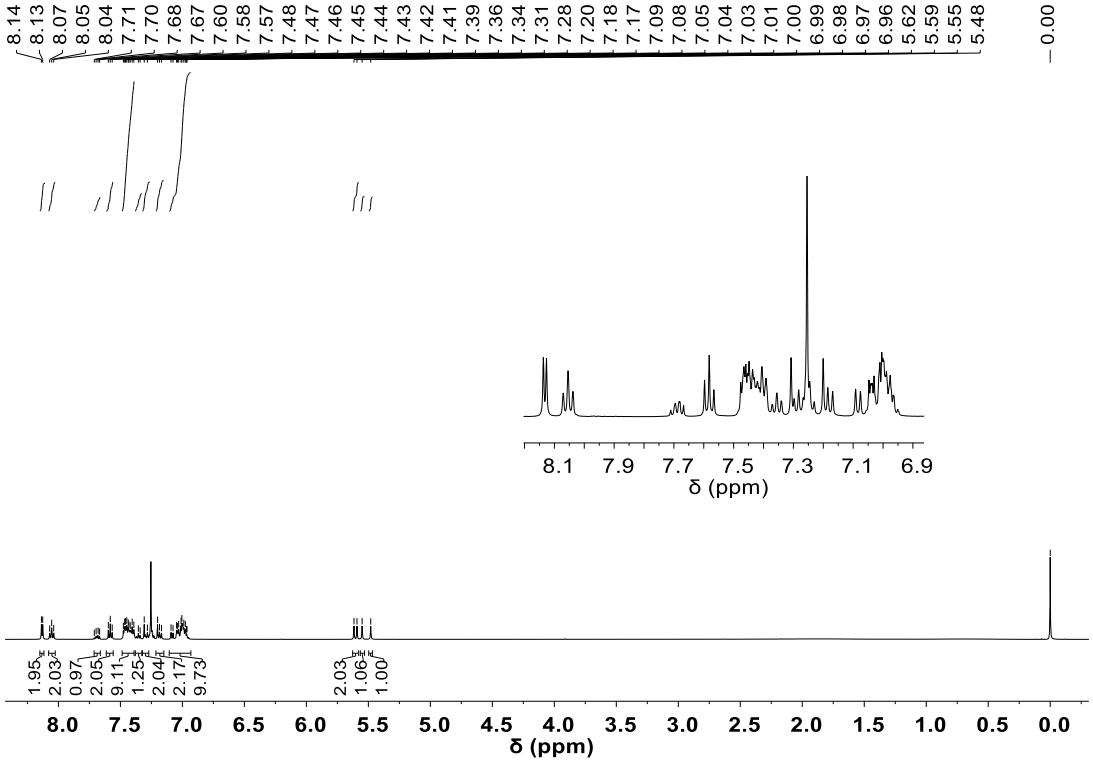

Fig. S1 ^{1}H NMR (500 MHz, $CDCl_3$, 298 K) of **TCz-Br**.

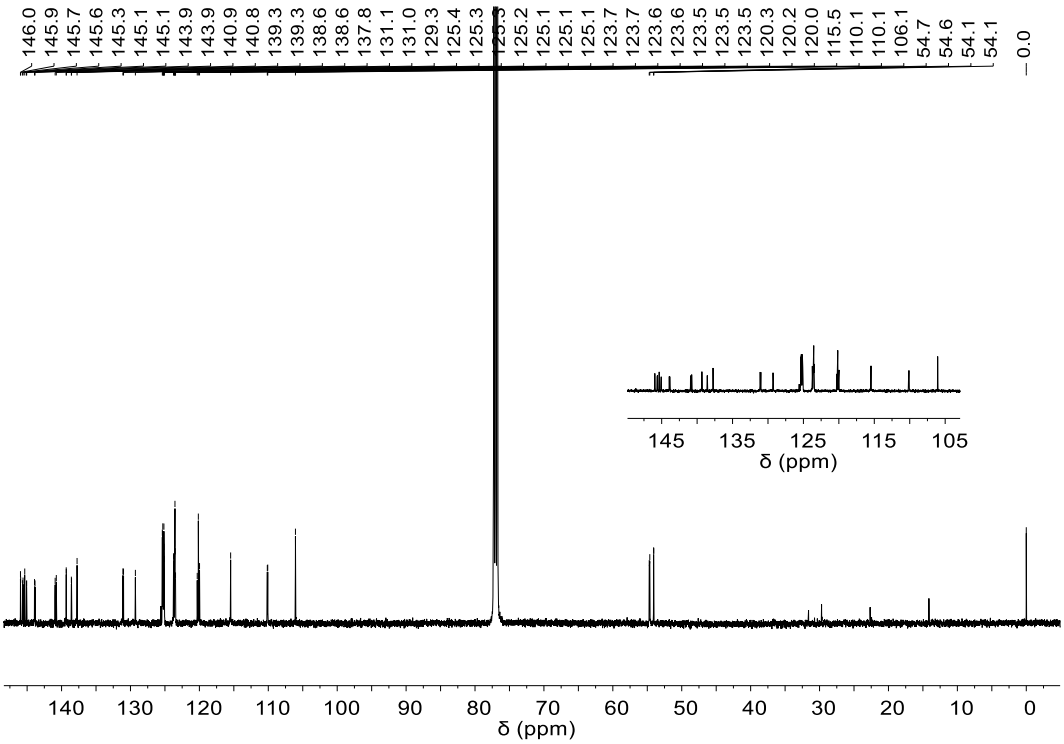

Fig. S2 ^{13}C NMR (126 MHz, $CDCl_3$, 298 K) of **TCz-Br**.

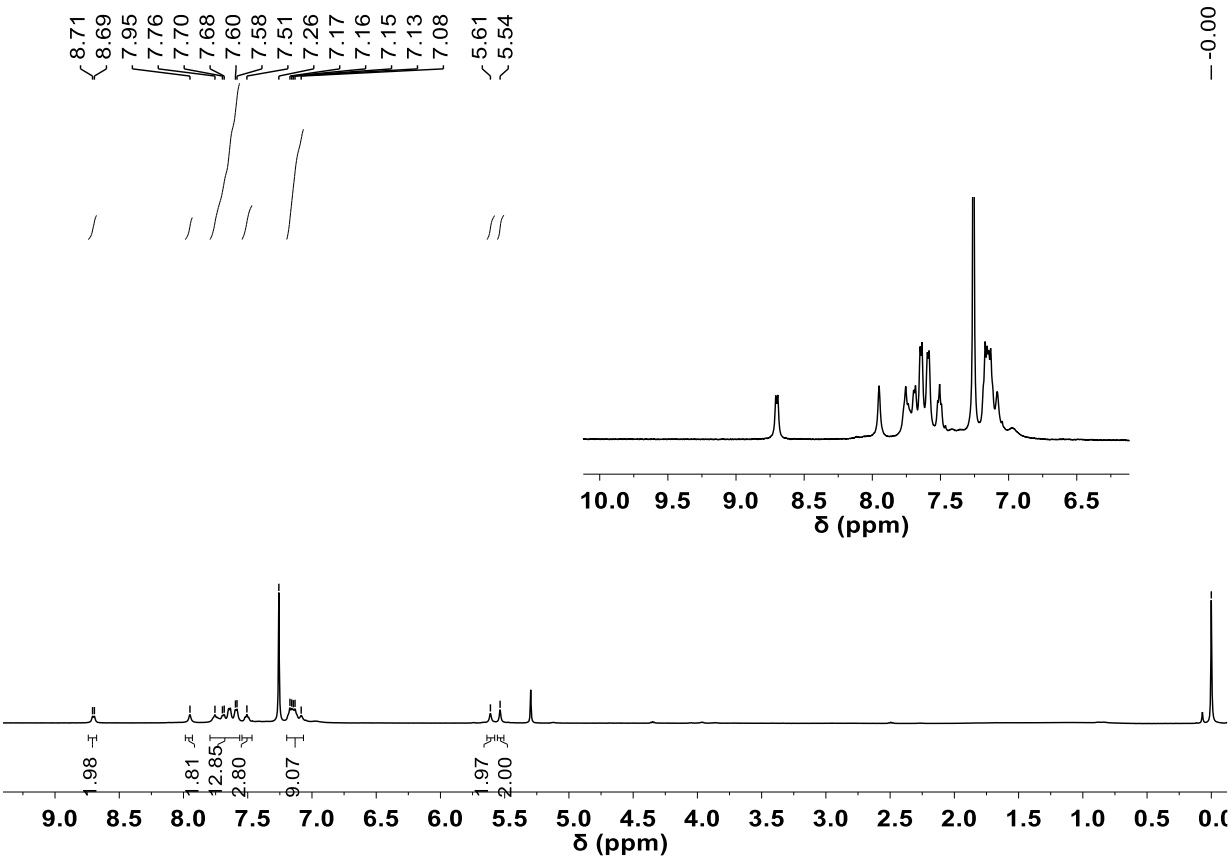

Fig. S3 ^{1}H NMR (500 MHz, $CDCl_3$, 298 K) of **TpBN**.

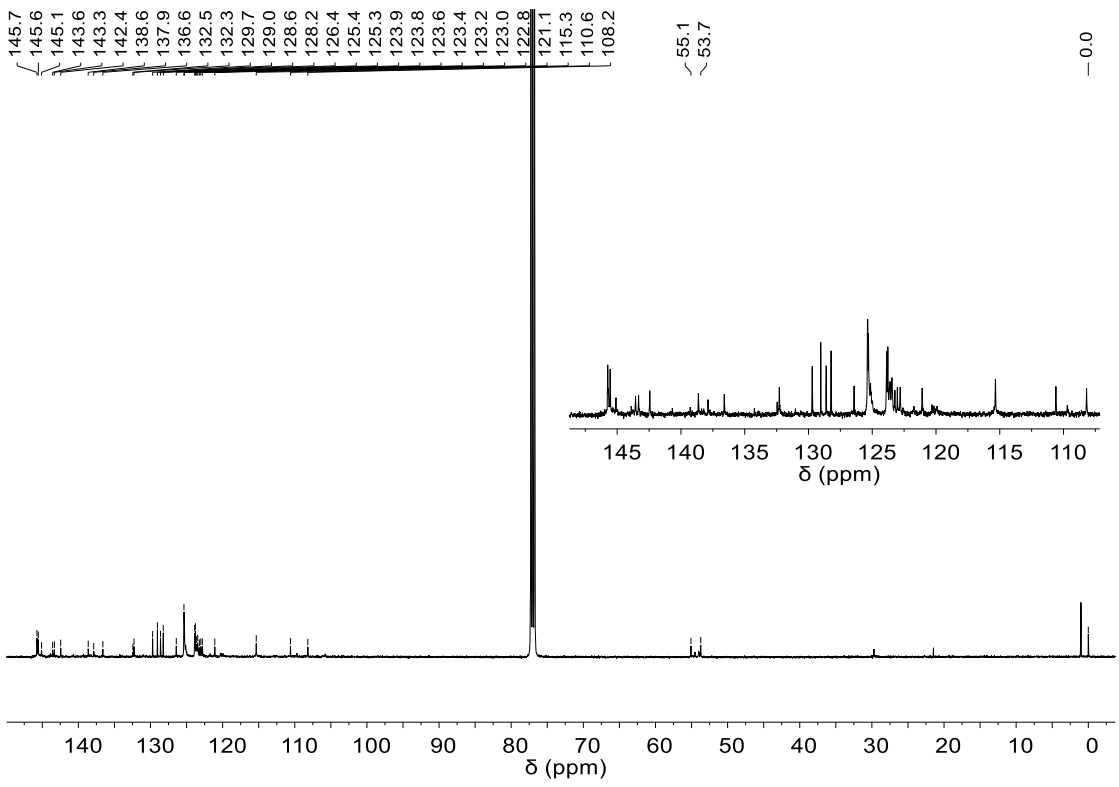

Fig. S4 ^{13}C NMR (125 MHz, $CDCl_3$, 298 K) of **TpBN**.

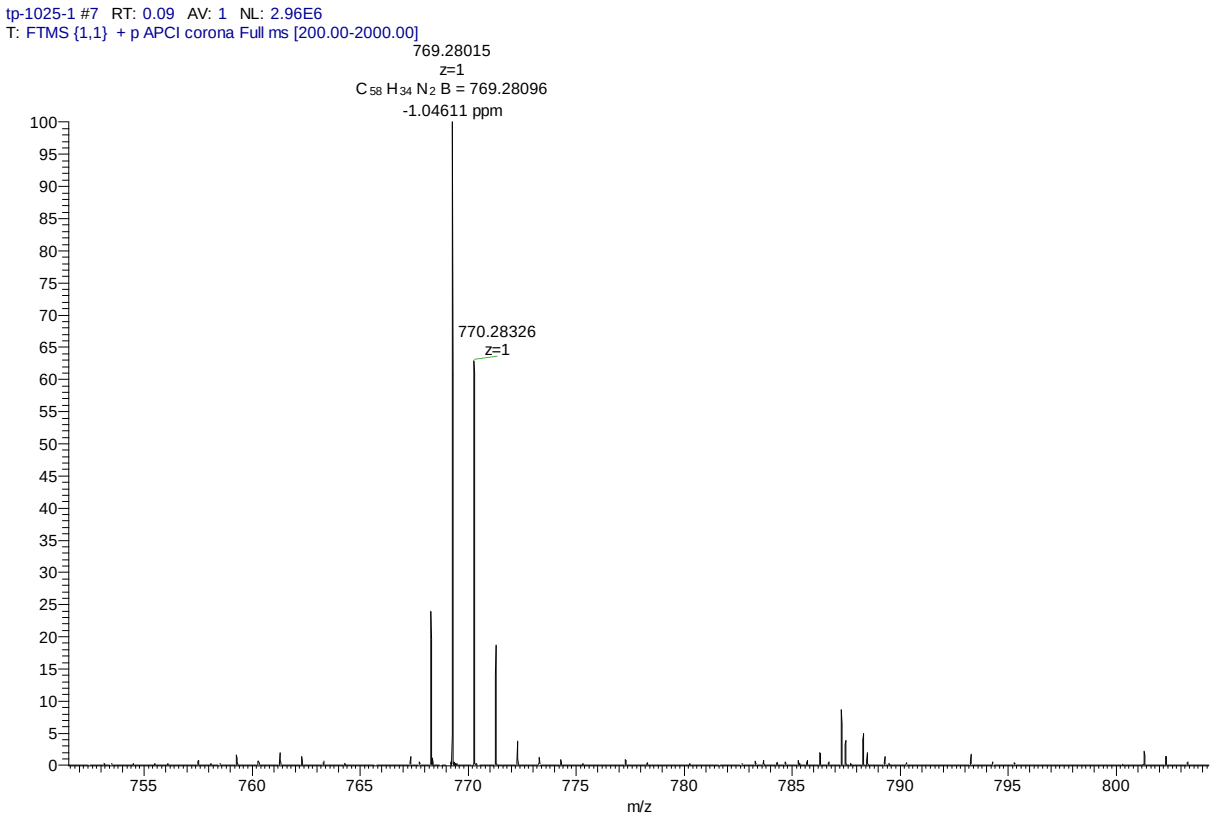

Fig. S5 HR-MS (APCI) of **TpBN**.

3. Electrochemical properties

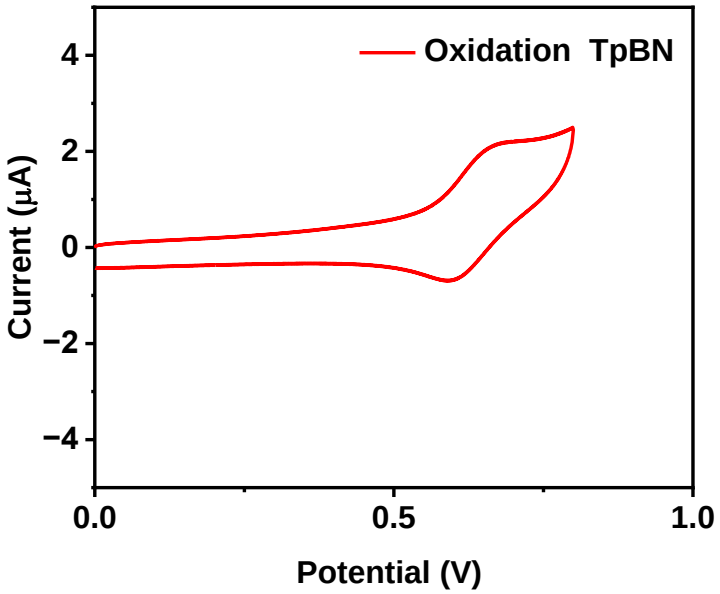

Fig. S6 Oxidation curve of cyclic voltammograms of **TpBN** measured in dichloromethane with 0.1 M tetra-*n*-butylammonium hexafluorophosphate.

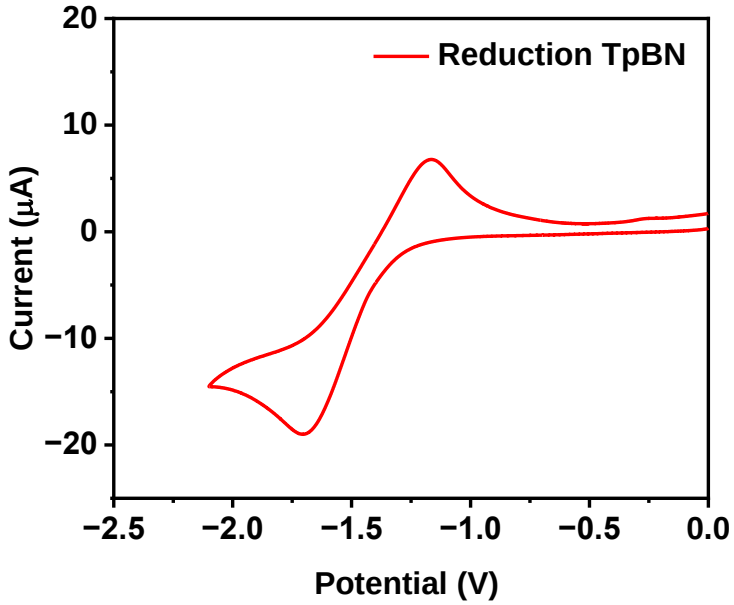

Fig. S7 Reduction curve of cyclic voltammograms of **TpBN** measured in THF with 0.1 M tetra-n-butylammonium hexafluorophosphate.

Table S1. Electrochemical properties of **TpBN**.

Compound	$E_{ox,\ onset}$ [V]	$E_{red,\ onset}$ [V]	HOMO[a] [eV]	LUMO[a] [eV]	E_g[b] [eV]
TpBN	0.56	-1.46	-5.22	-3.19	2.03

a) E_{HOMO} and E_{LUMO} calculated from the oxidation potential and reduction potential by cyclic voltammetry with ferrocene as the internal standard with the formula of $E_{HOMO} = -[E_{ox}-E_{(Fc/Fc+)}+4.8]$ eV and $E_{LUMO} = -[E_{red}-E_{(Fc/Fc+)}+4.8]$ eV.. b) Calculated with the formula of $E_g = E_{LUMO}-E_{HOMO}$.

4. Theoretical calculations

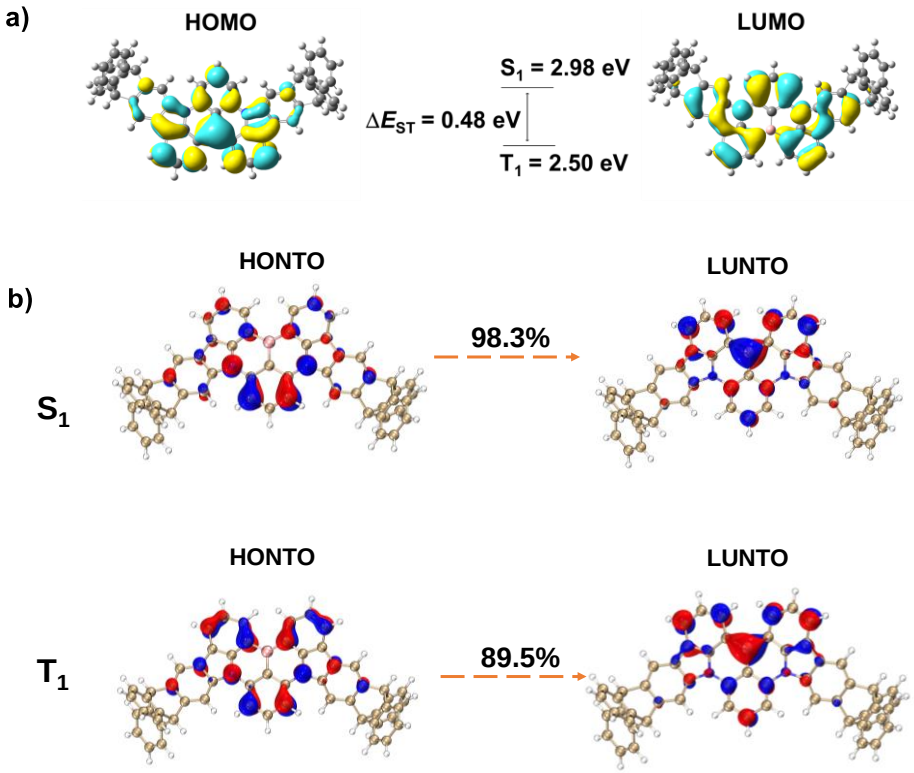

Fig. S8 a) Molecular orbitals and energy diagrams of **TpBN** calculated by TDDFT. b) Natural transition orbitals distributions and the state levels of **TpBN**.

5. Thermal properties

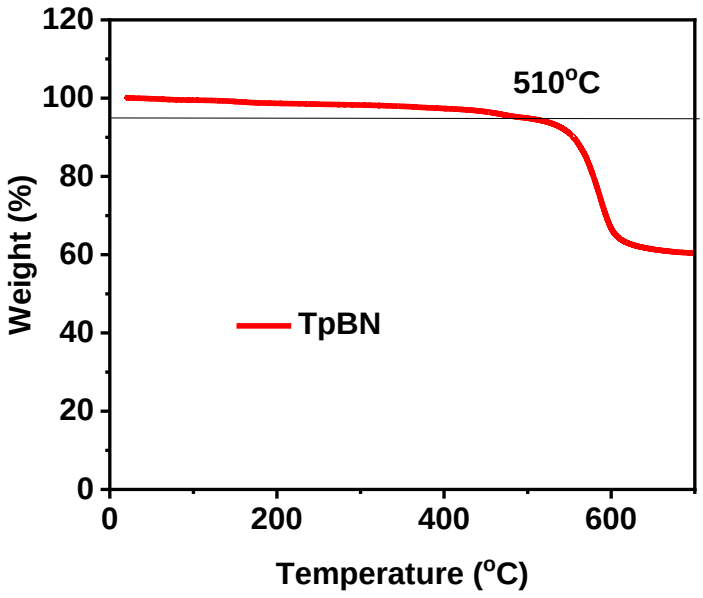

Fig. S9 TGA curves of **TpBN**.

6. Photophysical properties

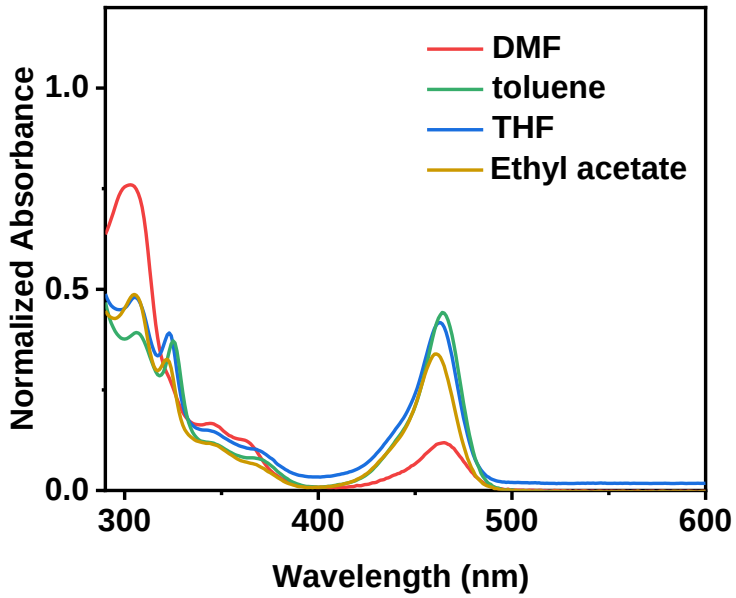

Fig. S10 UV-Vis absorption spectrum of **TpBN** in different solutions (c = 1.0 × 10^{-5} M).

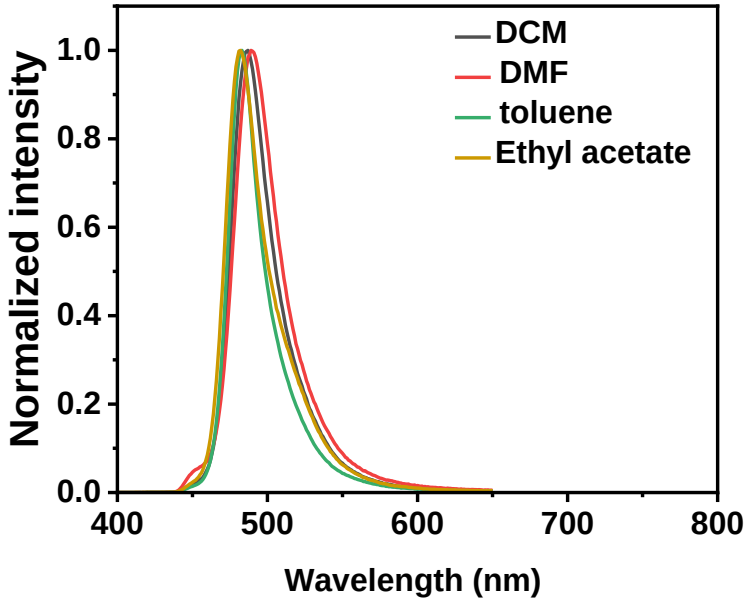

Fig. S11 PL spectrum of **TpBN** in different solutions (c = 1.0 × 10^{-5} M).

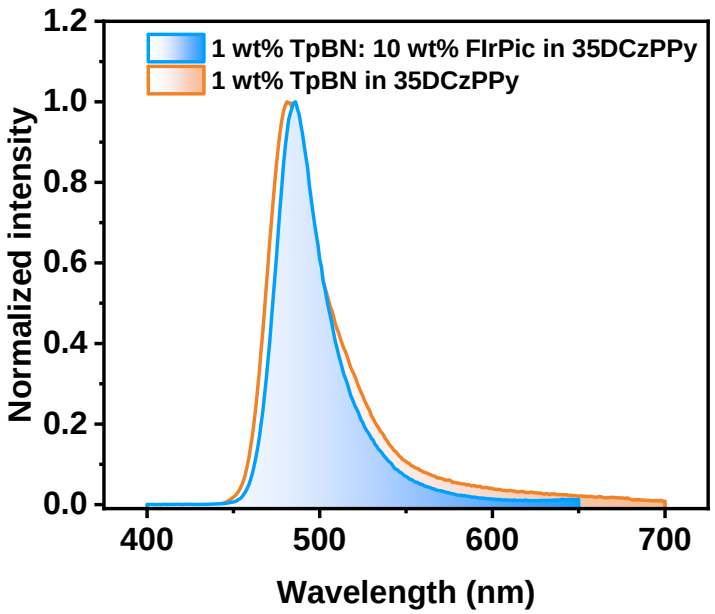

Fig. S12 PL spectrum of **TpBN** in doped films.

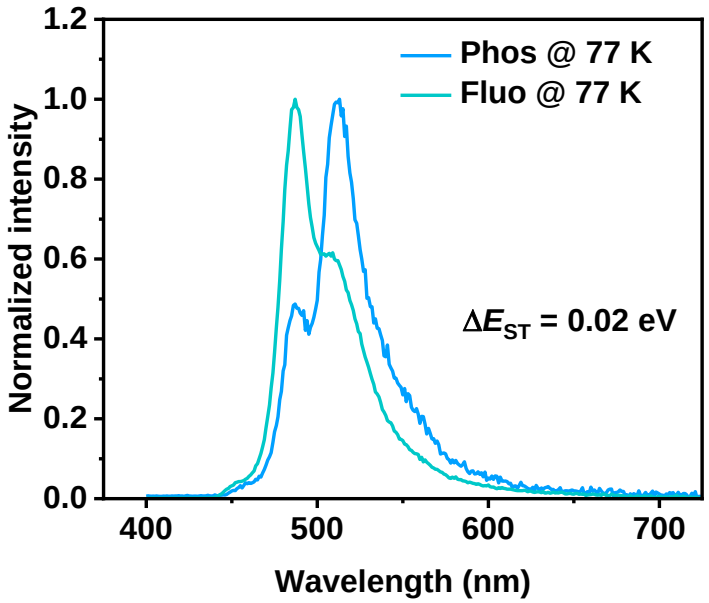

Fig. S13 Fluorescence and phosphorescence spectra of **TpBN** in doped films at 77 K.

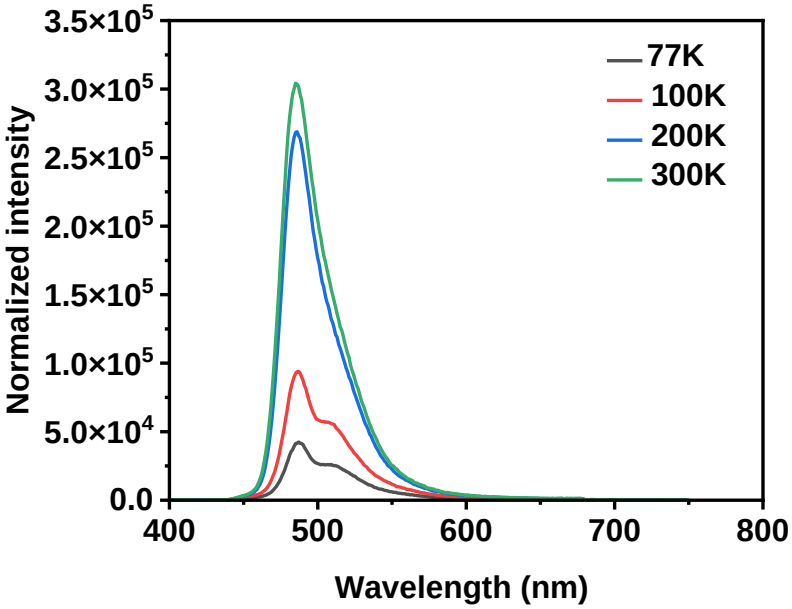

Fig. S14 PL spectrum of **TpBN** in doped film in different temperature.

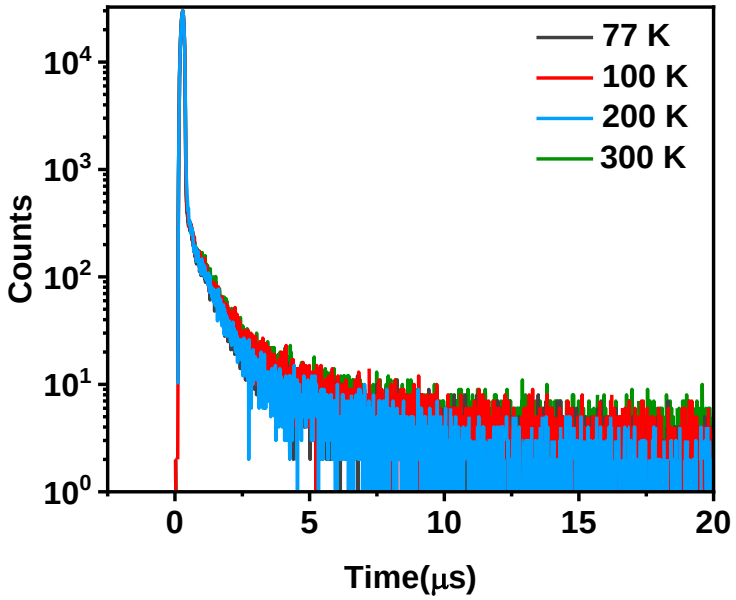

Fig. S15 Transient spectrum of **TpBN** in doped film in different temperature.

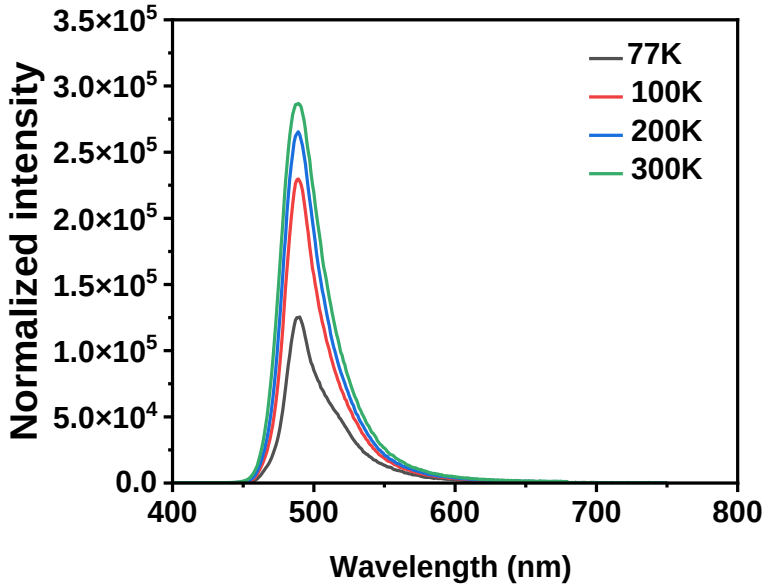

Fig. S16 Transient spectrum of **TpBN** in HF doped film in different temperature.

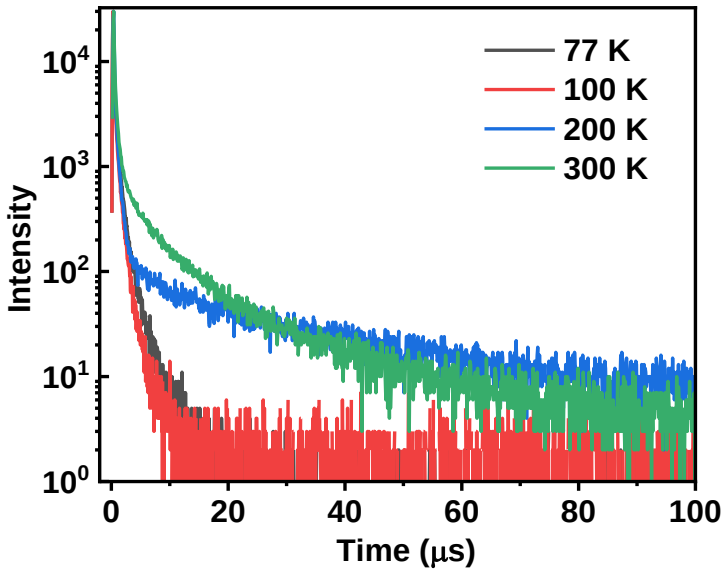

Fig. S17 Transient spectrum of **TpBN** in HF doped film in different temperature.

Scheme S2. The rate constants of intersystem crossing (k_{ISC}) and reverse intersystem crossing (k_{RISC}) of the emitter based on the following equations[S2]:

$k_p = \frac{\Phi_p}{\tau_p}$ k_p: Prompt fluorescence decay rate.

$k_d = \frac{\Phi_d}{\tau_d}$ k_d: Delayed fluorescence decay rate.

$\Phi_{PL} = \frac{k_p}{k_p + k_{IC}}$ k_{IC}: Internal conversion rate.

$k_{r,s} = k_p\Phi_p + k_d\Phi_d \approx k_p\Phi_p$ $k_{r,s}$: Radiative decay rate from a singlet excited state.

$k_{ISC} \approx (1 - \Phi_p)k_p$ k_{ISC}: Intersystem crossing rate.

$k_{RISC} \approx \frac{k_p k_d}{k_{ISC}} \cdot \frac{\Phi_d}{\Phi_p}$ k_{RISC}: Reverse intersystem crossing rate

Φ_{PL} is the absolute photoluminescence quantum yield; Φ_p is the prompt fluorescent component of Φ_{PL}; Φ_d is the delayed fluorescent component of Φ_{PL}.

According to the Fig. 2c, its luminescence decay can be fitted by double exponential method, with the lifetime of the delayed component (τ_{PF}) accounting for 69.59%.

Table S2. Photophysical characteristics of **TpBN**.

Molecule	λ_{abs} [nm]	λ_{FL} [nm]	PLQY [%]	FWHM	ΔE_{ST}[d] [eV]	τ_{PF}[b] [ns]	τ_{DF}[b] [μs]	k_{ISC} [x10^6]	k_{RISC} [x10^6]
TpBN	464[a]	480[a]/481[b]/486[C]	99.0[a]/94.0[b] /98.7[c]	28[a]/32[b] /31[c]	0.02	65	1.3	3.2	1.62

a) Measured in toluene at 298 K. b) Measured in doped film at 298 K. c) Measured in doped film with sensitizer. d) Measured in doped film at 77 K.

7. OLEDs performances

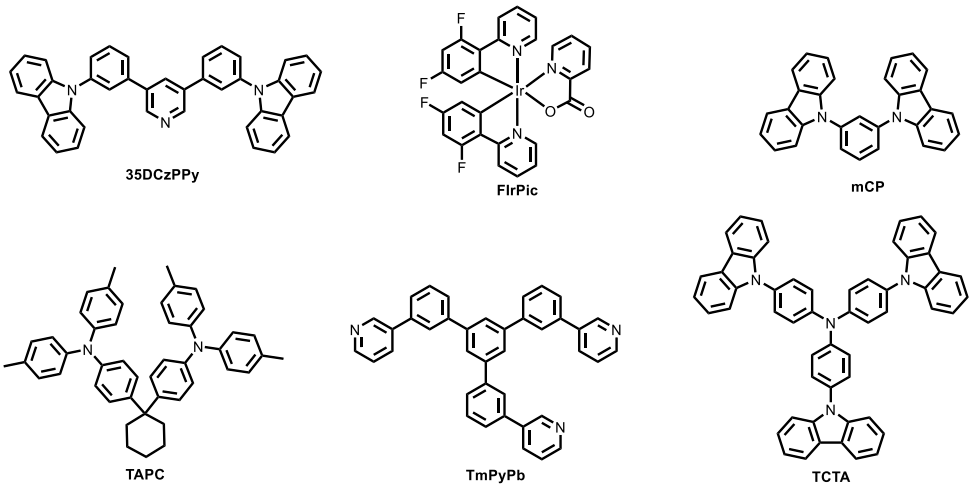

Fig. S18 Materials used for OLEDs based **TpBN**.

Table S3. EL performances of the OLEDs based on **TpBN**.

Device[a]	λ_{EL}[b] [nm]	FWHM[b] [nm]	CE[c] [cd A^{-1}]			PE[d] [lm W^{-1}]			EQE[e] [%]			Efficiency roll-off[f] (%)
			Max	1000 cd m^{-2}	5000 cdm^{-2}	Max	1000 cd m^{-2}	5000 cd m^{-2}	Max	1000 cd m^{-2}	5000 cdm^{-2}	
DA	488	36	58.3	52.3	44.7	52.3	32.8	23.4	27.0	24.7	21.3	8%
DB	486	34	47.3	43.0	34.8	42.2	37.0	16.8	23.0	21.3	17.2	7%

a) DA was the device based on **TpBN** in HF-OLEDs, DB was the device based on **TpBN** in non-sensitized OLEDs. b) The EL emission peak at 6 V. c) Maximum current efficiency and current efficiency with luminance at 1000 cd m^{-2} and 5000 cd m^{-2}. d) Maximum power efficiency and power efficiency with luminance at 1000 cd m^{-2} and 5000 cd m^{-2}. e) Maximum external quantum efficiency and external quantum efficiency with luminance at 1000 cd m^{-2} and 5000 cd m^{-2}. f) Efficiency roll-off at 1000 cd m^{-2}

Table S4. Summary of these MR-TADF materials based on triptycene skeleton

Material	λ_{max} (nm)	FWHM (nm)	Device	L_{max} (cd m^{-2})	EQE_{max} (%)	Ref.
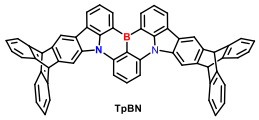 TpBN	486	32	OLED	27530	23.0	**This work**
			HF-OLED	41540	27.0	
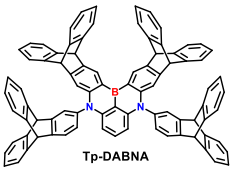 Tp-DABNA	458	24	OLED	-	24.3	*Angew. Chem. Int. Ed.* 2023, **62**, e202306879.
			HF-OLED	-	27.5	
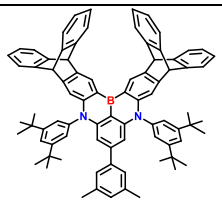 2,3-Tp-DABNA-xyl	472	21	OLED	-	25.7	*Chem. Eng. J.* 2024, **497**, 154839.
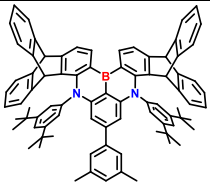 3,4-Tp-DABNA-xyl	467	27	OLED	-	25.9	
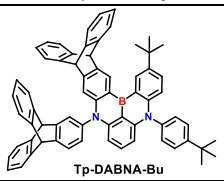 Tp-DABNA-Bu	460	30	No electroluminescence properties reported			*Bull. Korean Chem. Soc*. 2025, **46**, 171.
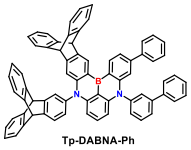 Tp-DABNA-Ph	474	39				
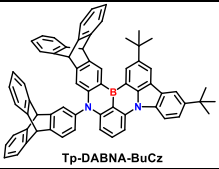 Tp-DABNA-BuCz	474	32				

Computational geometry data

Geometrically optimized Cartesian coordinates in Å

C	-6.44061	-2.07564	0.408
C	-7.44663	-1.66706	1.4698
C	-8.27665	-0.61846	1.05987
C	-7.97022	-0.1379	-0.34802
C	-7.25328	-2.41175	-0.83035
C	-8.08246	-1.36201	-1.23958
C	-6.49932	0.2395	-0.34284
C	-5.66601	-0.81607	0.06023
C	-4.29234	-0.67875	0.13162
C	-3.74112	0.55458	-0.22674
C	-4.58097	1.63673	-0.5734
C	-5.96476	1.47404	-0.64343
C	-9.24939	-0.124	1.90953
C	-9.39432	-0.68207	3.18012
C	-8.57029	-1.72271	3.58694
C	-7.5891	-2.22079	2.72901
C	-7.23154	-3.60169	-1.5348
C	-8.04624	-3.74513	-2.65837
C	-8.86942	-2.70353	-3.06457
C	-8.89018	-1.50335	-2.35326
N	-2.40697	1.0078	-0.2252
C	-2.42432	2.37325	-0.4638
C	-3.73866	2.79658	-0.72498
C	-1.32173	3.22682	-0.41374
C	-1.59305	4.56879	-0.72932
C	-2.87666	5.01046	-1.0349
C	-3.96169	4.13366	-1.02035

C	-1.19323	-1.09988	-0.20243
C	-0.00004	-1.77185	-0.0002
C	1.19316	-1.09991	0.20211
C	1.21053	0.29356	0.13346
C	-0.00001	1.02788	-0.00005
C	-1.21056	0.29359	-0.13363
C	6.44066	-2.07559	-0.40818
C	7.25323	-2.41184	0.83021
C	8.08237	-1.36215	1.23962
C	7.9702	-0.13793	0.34818
C	7.44677	-1.6669	-1.46985
C	8.27676	-0.61834	-1.05973
C	6.49931	0.23947	0.34291
C	5.66603	-0.81606	-0.06033
C	4.29236	-0.67874	-0.13182
C	3.7411	0.55454	0.22666
C	4.58093	1.63666	0.57348
C	5.96472	1.47397	0.6436
C	8.88998	-1.5036	2.35336
C	8.86915	-2.70385	3.06455
C	8.04601	-3.7454	2.65816
C	7.23141	-3.60185	1.53453
C	7.58936	-2.2205	-2.72911
C	8.57064	-1.72233	-3.58688
C	9.39462	-0.68173	-3.17988
C	9.24958	-0.1238	-1.90925
N	2.40695	1.00776	0.22509
C	2.42429	2.37319	0.46382
C	3.73862	2.79649	0.72511
C	1.32171	3.22678	0.41377

C	1.59303	4.56872	0.72948
C	2.87662	5.01036	1.03516
C	3.96164	4.13355	1.02059
B	-0.00001	2.56574	0.
H	-5.79496	-2.89618	0.72771
H	-8.6167	0.68193	-0.66745
H	-3.69663	-1.49897	0.50712
H	-6.60484	2.30975	-0.91231
H	-9.89357	0.69089	1.59048
H	-10.15545	-0.29936	3.85318
H	-8.68849	-2.15167	4.57728
H	-6.94323	-3.0349	3.04665
H	-6.58713	-4.41641	-1.21563
H	-8.03551	-4.67623	-3.2167
H	-9.50056	-2.82209	-3.94002
H	-9.53385	-0.6875	-2.6708
H	-0.77558	5.2818	-0.75333
H	-3.03934	6.05587	-1.27801
H	-4.96246	4.49484	-1.23871
H	-2.0836	-1.66159	-0.43696
H	-0.00005	-2.85773	-0.00025
H	2.08352	-1.66167	0.43658
H	5.79504	-2.8961	-0.72804
H	8.61666	0.68186	0.66775
H	3.6967	-1.49891	-0.50747
H	6.60478	2.30965	0.91261
H	9.53363	-0.68778	2.67105
H	9.50021	-2.8225	3.94005
H	8.03522	-4.67656	3.2164
H	6.58703	-4.41654	1.21521

H	6.94352	-3.03457	-3.04688
H	8.68893	-2.15119	-4.57726
H	10.15582	-0.29895	-3.85283
H	9.89373	0.69106	-1.59006
H	0.77556	5.28173	0.7535
H	3.03929	6.05575	1.27835
H	4.9624	4.4947	1.23904

References:

S1. Gaussian 09, Revision D.01, M. J. Frisch, G. W. Trucks, H. B. Schlegel, G. E. Scuseria, M. A. Robb, J. R. Cheeseman, G. Scalmani, V. Barone, B. Mennucci, G. A. Petersson, H. Nakatsuji, M. Caricato, X. Li, H. P. Hratchian, A. F. Izmaylov, J. Bloino, G. Zheng, J. L. Sonnenberg, M. Hada, M. Ehara, K. Toyota, R. Fukuda, J. Hasegawa, M. Ishida, T. Nakajima, Y. Honda, O. Kitao, H. Nakai, T. Vreven, J. A. Montgomery, Jr., J. E. Peralta, F. Ogliaro, M. Bearpark, J. J. Heyd, E. Brothers, K. N. Kudin, V. N. Staroverov, T. Keith, R. Kobayashi, J. Normand, K. Raghavachari, A. Rendell, J. C. Burant, S. S. Iyengar, J. Tomasi, M. Cossi, N. Rega, J. M. Millam, M. Klene, J. E. Knox, J. B. Cross, V. Bakken, C. Adamo, J. Jaramillo, R. Gomperts, R. E. Stratmann, O. Yazyev, A. J. Austin, R. Cammi, C. Pomelli, J. W. Ochterski, R. L. Martin, K. Morokuma, V. G. Zakrzewski, G. A. Voth, P. Salvador, J. J. Dannenberg, S. Dapprich, A. D. Daniels, O. Farkas, J. B. Foresman, J. V. Ortiz, J. Cioslowski, D. J. Fox, Gaussian, Inc., Wallingford CT, 2013.

S2. K. Goushi, K. Yoshida, K. Sato, C. Adachi, *Nature Photon*., 2012, **6**, 253.